Freezing in the presence of disorder: a lattice study

2003 J. Phys.: Condens. Matter 15 4695

(http://iopscience.iop.org/0953-8984/15/27/304)

INSTITUTE OF PHYSICS PUBLISHING JOURNAL OF PHYSICS: CONDENSED MATTER

J. Phys.: Condens. Matter **15** (2003) 4695–4708 PII: S0953-8984(03)58678-7

Freezing in the presence of disorder: a lattice study

Matthias Schmidt[1,3], **Luis Lafuente**[2] **and José A Cuesta**[2]

[1] Soft Condensed Matter, Debye Institut, Utrecht University, Princetonpln 5, 3584 CC Utrecht, The Netherlands
[2] Grupo Interdisciplinar de Sistemas Complejos (GISC), Departamento de Matemáticas, Universidad Carlos III de Madrid, Avenida de la Universidad 30, 28911 Leganés, Madrid, Spain

E-mail: mschmidt@thphy.uni-duesseldorf.de

Received 22 January 2003
Published 27 June 2003
Online at stacks.iop.org/JPhysCM/15/4695

Abstract

We investigate the freezing transition in a two-dimensional lattice model of annealed hard squares that are subject to the influence of randomly placed quenched particles of the same size. The latter model is a porous medium. By combining two recent density functional approaches we arrive at a theory for quenched–annealed lattice fluids that treats the quenched particles on the level of their one-body density distribution. We show that this approach yields thermodynamics that compare well with results from treating matrix realizations explicitly and performing subsequent averaging over the disorder. The freezing transition from a fluid to a columnar phase is found to be continuous. On increasing matrix density it shifts towards close packing and vanishes beyond a threshold matrix density.

1. Introduction

Ordering phenomena, like the freezing transition, in the presence of disorder [1] and confinement [2] are genuinely interesting, as self-organization competes with external constraints. Much work has been devoted to understand liquid condensation in porous media—for recent work see e.g. [3–5], where insight was gained into hysteresis in sorption curves and its relation to the occurrence of a complex free-energy landscape. However, generally speaking the freezing transition under confinement is not as well understood as in the bulk. Thalmann *et al* [6] have investigated a hard sphere fluid in a random pinning potential, finding that the first-order crystallization transition of the pure fluid changes to a continuous glass transition as the strength of the disorder is increased above a critical value. For the same system, Dasgupta and Valls [7] have mapped out regions in the phase diagram corresponding to liquid, glassy and crystalline states. As a theoretical toy one often models disordered, amorphous matrices

[3] On leave from: Institut für Theoretische Physik II, Heinrich-Heine-Universität Düsseldorf, Universitätsstraße 1, D-40225 Düsseldorf, Germany.

by quenched (immobilized) configurations of a (model) fluid. Then the adsorbate is annealed (allowed to equilibrate) in the presence of the matrix particles that act as an external potential.

In this work we study freezing in porous media by combining two recent density functional techniques [8], both of which originate from Rosenfeld's fundamental measure theory (FMT) [9], and construct the functional from the zero-dimensional (0D) limit [10]. The first technique is lattice fundamental measure theory (LFMT), which is the generalization of continuum FMT to lattice models [11, 12]. The second technique is a formulation of density functional theory (DFT) where the functional gives directly the free energy averaged over matrix realizations [13]; we refer to this approach as a quenched–annealed (QA) DFT, as the free-energy functional operates on density profiles of both quenched and annealed species. These approaches have been tested before in some situations. In particular, the latter produces results for fluid demixing and liquid structure that compare well with those from integral equation approaches [14]. The comprehensible structure of FMT allows us to derive a DFT for QA lattice fluids. The main motivation for considering such an approach is the computational simplicity of the lattice model over the continuum model. On the lattice it is practical (as will be shown below) to also consider the matrix explicitly as an external potential and minimize the inhomogeneous adsorbate density profile. In the continuum case this would be a daunting task (although some progress has been reported [15]). In essence we follow the same strategy as that in [3–5], albeit not for liquid condensation but for an ordering phase transition. Despite the fact that our main concern is the study of equilibrium properties, we have also checked for the presence of out-of-equilibrium hysteresis in the sorption isotherms.

Hard-body systems provide a paradigm in the study of freezing within statistical mechanics. The simplicity introduced by lattice models, compared to continuum models, led many authors to use them to investigate the liquid–solid transition [16]. Since hard-body systems have no interaction energy in any admissible configuration, the driving force of phase transitions is entropy alone. Thus, calculating the partition function of such systems amounts to counting the number of allowed microscopic configurations compatible with a certain macroscopic state (in a one-component system determined by the density or the fugacity). This task can only be performed in an exact manner for a few models, thus approximate schemes are needed in order to deal with a broad range of models. The most successful theories in this respect are based on combinatorial facts, however this makes the calculation of an approximate entropy a daunting task [17]. The theory we use in this work (LFMT) [12] has the advantage of circumventing the counting task and producing a closed-form density functional from which the thermodynamics and structure can be extracted through the standard routes of DFT. Furthermore, the results obtained are of the same level of accuracy as those produced by the classical approaches [11].

As a simple model for both the adsorbate and the matrix species we use two-dimensional hard square particles. This is just the lattice gas with nearest- and second-nearest-neighbour exclusion on the simple square lattice. This system has been studied before [18–21] but no definitive conclusion has been reached about its phase behaviour. Some authors have claimed it to have a second-order transition [18, 20], others a weaker (third-order) transition [18, 21] and others even no transition at all [18–20]. The only thing that seems clear is the structure near close packing: periodic along one coordinate axis while uniform along the other (i.e. columnar). The period of the density oscillation equals the particle size. The FMT also predicts the columnar phase to be stable and a continuous fluid–columnar transition [12].

We add freely overlapping matrix particles and describe their influence via two different routes. First, we model the matrix as an external potential and minimize the functional explicitly. This is a straightforward application of the equilibrium LFMT; we refer to this as the external potential method. Second, we use the QA DFT and compare results for

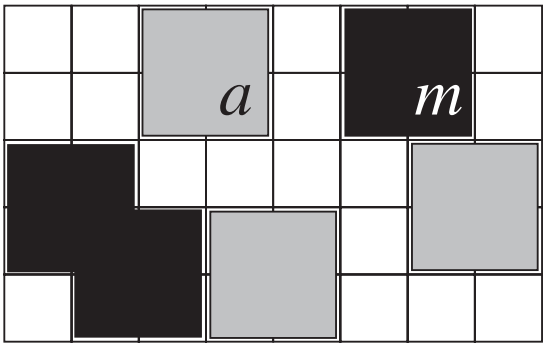

Figure 1. Illustration of the lattice model of adsorbate square particles (grey, species a) and matrix square particles (black, species m) on a two-dimensional cubic lattice. The adsorbate–adsorbate and adsorbate–matrix interactions are hard core; the matrix–matrix interaction is ideal.

thermodynamic quantities, where we find reasonably good agreement over a broad range of densities in the fluid phase. Hence we trust the results for the phase diagram of the QA DFT. This indicates that the fluid–columnar transition remains continuous in the presence of disorder. On increasing the matrix density, the critical density shifts towards close packing and the ordered phase ceases to exist beyond a certain threshold value (very close to the percolation threshold of the matrix).

We do not find any signs for the occurrence of hysteresis in sorption curves, i.e. the same results for the adsorption are obtained whether increasing or decreasing the adsorbate fugacity. We speculate that this is due to the fact that the underlying equilibrium phase transition is continuous.

This paper is organized as follows. We define the lattice hard-body model in section 2. In section 3 we describe both density functional approaches (the details of the derivation of the QA DFT are given in the appendix). Section 4 is devoted to the thermodynamics and phase behaviour, and we conclude in section 5.

2. Model

As an adsorbate we consider square hard-core particles (species a) on a two-dimensional square lattice (with unit-length lattice spacing) that interact by means of a pair potential as a function of the relative distance vector $\boldsymbol{s}$ of particle centres given by

$$V_{aa}(\boldsymbol{s}) = \begin{cases} \infty & \text{if } |s_x| < 2 \text{ and } |s_y| < 2, \\ 0 & \text{otherwise.} \end{cases} \tag{1}$$

The adsorbate is subject to the influence of a porous matrix that is modelled by freely overlapping particles (species m) of the same shape as the adsorbate particles. Then the interaction between matrix and adsorbate particles is also $V_{am}(\boldsymbol{s}) = V_{aa}(\boldsymbol{s})$. As the matrix consists of freely overlapping particles, it is just an ideal gas, hence $V_{mm}(\boldsymbol{s}) = 0$. Figure 1 shows a sketch of the model. Notice that ideality of the matrix implies the possibility of multiple occupancy of lattice sites.

We denote the one-body distributions of adsorbate and matrix particles by $\rho_a(\boldsymbol{s})$ and $\rho_m(\boldsymbol{s})$, respectively, and the fugacity of the adsorbate particles by z_a.

3. Theory

3.1. Matrix as an external potential

The grand potential functional (in fact a function of the density at the lattice sites) for the system is expressed as

$$\Omega[\rho_a] = F_{id}[\rho_a] + F_{exc}[\rho_a] + \sum_{\boldsymbol{s}\in\mathbb{Z}^2} \rho_a(\boldsymbol{s})[V_{ext}^{rand}(\boldsymbol{s}) + V_{ext}^{misc}(\boldsymbol{s}) - \mu_a], \tag{2}$$

where $\mu_a = k_B T \ln z_a$ is the adsorbate chemical potential, $k_B T$ being the Boltzmann constant multiplied by the absolute temperature. We have split the external potential into two parts: $V_{ext}^{rand}(\boldsymbol{s})$ models the presence of the matrix particles; $V_{ext}^{misc}(\boldsymbol{s})$ is a possible additional contribution such as a gravitational field. (In the following we will restrict ourselves to situations where $V_{ext}^{misc} = 0$.) The ideal free-energy functional in equation (2) is given by

$$F_{id}[\rho_a] = k_B T \sum_{\boldsymbol{s}\in\mathbb{Z}^2} \rho_a(\boldsymbol{s}) \ln[\rho_a(\boldsymbol{s}) - 1]. \tag{3}$$

Following the recent extension of FMT to lattices [11, 12], the excess free-energy functional is approximated as

$$F_{exc}[\rho_a] = k_B T \sum_{\boldsymbol{s}\in\mathbb{Z}^2} [\Phi_0(\square_a) - \Phi_0(\vert_a) - \Phi_0(\circ\!-\!\circ_a) + \Phi_0(\circ_a)], \tag{4}$$

where the exact 0D excess free energy as a function of the mean number of adsorbate particles, η_a, is

$$\Phi_0(\eta_a) = (1 - \eta_a)\ln(1 - \eta_a) + \eta_a. \tag{5}$$

The arguments in equation (4) are weighted densities, for which we use a diagrammatic notation [22]: each circle corresponds to the density at a lattice point and lines indicate lattice spacings; the subscript i indicates the species (here only a). More explicitly, the weighted densities for species i are given as

$$\square_i = \rho_i(s_x, s_y) + \rho_i(s_x + 1, s_y) + \rho_i(s_x, s_y + 1) + \rho_i(s_x + 1, s_y + 1), \tag{6}$$

$$\vert_i = \rho_i(s_x, s_y) + \rho_i(s_x, s_y + 1), \tag{7}$$

$$\circ\!-\!\circ_i = \rho_i(s_x, s_y) + \rho_i(s_x + 1, s_y), \tag{8}$$

$$\circ_i = \rho_i(s_x, s_y). \tag{9}$$

As usual in DFT for one-component systems, the equilibrium condition is

$$\frac{\delta\Omega[\rho_a]}{\delta\rho_a(\boldsymbol{s})} = 0, \tag{10}$$

from which the equilibrium density profile and grand potential are obtained once a matrix realization V_{ext}^{rand} is prescribed.

The average over different matrix realizations is performed subsequently. In practice we use a two-dimensional lattice of 64×64 sites with periodic boundary conditions. A realization of the external potential is generated by randomly placing matrix particles on the lattice:

$$V_{ext}^{rand}(\boldsymbol{s}) = \sum_{\boldsymbol{s}'\in M} V_{am}(\boldsymbol{s} - \boldsymbol{s}'), \tag{11}$$

where M is a set of random lattice sites. Clearly, this yields a discrimination into forbidden and allowed lattice sites. Then, for a given adsorbate fugacity z_a, the Euler–Lagrange equation (10) is solved by a simple iteration procedure. From the converged solution both the grand potential, $\beta\Omega$, where $\beta = 1/(k_B T)$, and the density of the adsorbate, ρ_a, are obtained. This procedure is carried out multiple times and a subsequent average over the disorder is taken. We use 50 independent matrix realizations, which we find to be sufficient.

3.2. *Quenched–annealed density functional theory*

Here we express the grand potential of the adsorbate in the presence of the quenched matrix particles as

$$\Omega[\rho_m;\,\rho_a] = F_{id}[\rho_a] + F_{exc}[\rho_m;\,\rho_a] + \sum_{\boldsymbol{s}\in\mathbb{Z}^2} \rho_a(\boldsymbol{s})[V_{ext}^{misc}(\boldsymbol{s}) - \mu_a]. \tag{12}$$

This functional is to be minimized only with respect to the adsorbate component,

$$\left.\frac{\delta\Omega[\rho_m;\,\rho_a]}{\delta\rho_a(\boldsymbol{s})}\right|_{\rho_m} = 0, \tag{13}$$

while the matrix density field, $\rho_m(\boldsymbol{s})$, is kept fixed. We remark that the structure of equations (12) and (13) is different from that of DFT for fully annealed systems, whether pure or binary. Although the first and third term on the right-hand side of equation (12) also appear in a one-component theory for ρ_a, the dependence of the excess free energy (second term on the right-hand side of equation (12)) on ρ_m is absent in such a treatment (see equation (2)). In the theory for a fully annealed (equilibrium) binary system, minimization would be required not only with respect to ρ_a but also with respect to ρ_m.

Furthermore, the excess free energy in the current treatment has a fundamentally different meaning to that of the equilibrium case. It includes not only the adsorbate–adsorbate interactions but also the interactions between (annealed) adsorbate and (quenched) matrix particles. It is an approximation for the free energy *averaged* over matrix realizations. As an aside, it differs (in general, but not necessarily) from the free energy of a corresponding equilibrium system, where the matrix is annealed rather than quenched.

Since (12) is a disorder-averaged grand potential, the meaning of the $\rho_a(\boldsymbol{s})$ resulting from equation (13) differs from that of the solution of equation (10): the latter represents the equilibrium density profile for a given realization of the matrix and will be non-uniform even in fluid phases; the former is an average density profile over matrix realizations and will be uniform in fluid phases.

In [13] the functional $F_{exc}[\rho_m;\,\rho_a]$ was obtained by first computing the exact excess free energy of a continuum system in a 0D cavity (i.e. one that is so small that all particles inside overlap) and then applying a general procedure to obtain a fundamental measure functional in three dimensions. As equation (4) reflects, a similar procedure to pass from 0D to higher dimensions exists for lattice models [12], which involves evaluating the 0D functional, Φ_0, for a certain set of 0D cavities (the diagrams (6)–(9)). The derivation of Φ_0 for those cavities in the presence of matrix particles and the subsequent construction of the functional is deferred to the appendix. We quote here that the final functional for an ideal matrix has the form

$$F_{exc}[\rho_m;\,\rho_a] = k_BT \sum_{\boldsymbol{s}\in\mathbb{Z}^2} [\Phi_0(\,;\,) - \Phi_0(\,;\,) - \Phi_0(\,;\,) + \Phi_0(\,;\,)], \tag{14}$$

where the weighted densities are defined in equations (6)–(9) and Φ_0 is a function of the mean numbers of matrix particles, η_m, and adsorbate particles, η_a, given by

$$\Phi_0(\eta_m;\,\eta_a) = (\mathrm{e}^{-\eta_m} - \eta_a)\ln(\mathrm{e}^{-\eta_m} - \eta_a) + \eta_a + \eta_m\mathrm{e}^{-\eta_m}. \tag{15}$$

In what follows we will be concerned with homogeneous matrices, i.e. those for which $\rho_m(\boldsymbol{s}) =$ constant. This allows us to evaluate the functional (12) and obtain analytical results. Hence, as could already be anticipated from the overall structure, this approach is computationally much simpler than that of the external potential method in section 3.1.

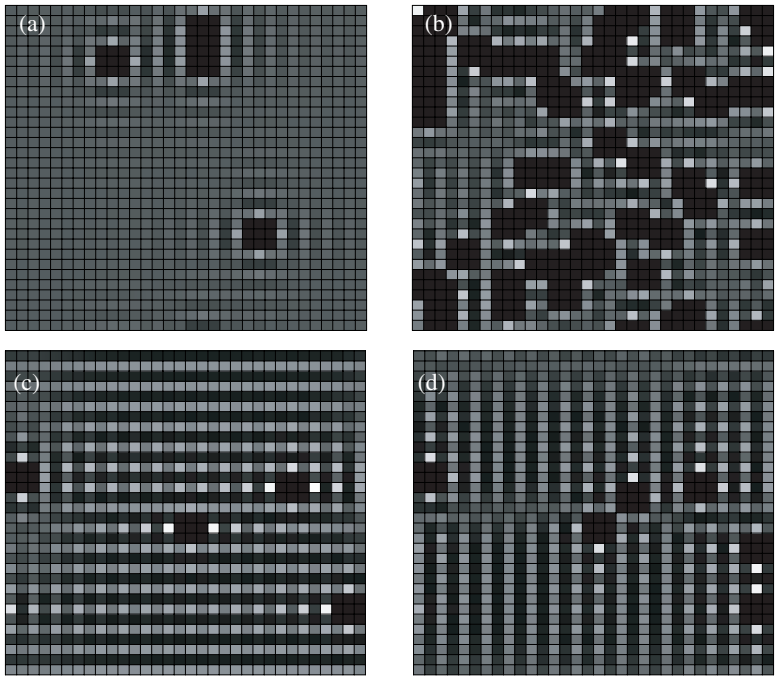

Figure 2. The density profile of the hard square adsorbate in a porous medium. Bright (dark) colours correspond to high (low) values of adsorbate density, ρ_a; black squares indicate lattice sites that are forbidden due to matrix particles. Fluid (a), (b) and columnar (c), (d) configurations are shown. Adsorbate fugacities and matrix densities are: (a) $z_a = 4$, $\rho_m = 0.003\,91$; (b) $z_a = 4$, $\rho_m = 0.050\,78$; (c) $z_a = 16$, $\rho_m = 0.003\,91$; and (d) $z_a = 16$, $\rho_m = 0.007\,82$. These snapshots are from lattices with 32×32 sites; the results presented are obtained with 64×64 sites.

4. Results

4.1. Thermodynamics

We start by comparing, over a broad range of densities of both adsorbate and matrix particles, the results from the QA DFT (section 3.2) with those from treating the matrix as an external potential (section 3.1). This serves as a benchmark to assess the accuracy of the QA DFT.

As an illustration, we plot the adsorbate density profiles, $\rho_a(\boldsymbol{s})$, in figure 2. For clarity we used a smaller system with 32×32 sites. Fluid configurations for low (a) and moderate (b) matrix densities are shown. As expected, the matrix causes inhomogeneities in the adsorbate density profile. For small ρ_m this is only a weak perturbation, but for larger ρ_m a highly irregular distribution results.

We first consider the change in grand potential due to the presence of the matrix. In particular, we consider the change in grand potential per matrix particle, $\beta[\Omega(\rho_m) - \Omega(\rho_m = 0)]/N_m$, where N_m is the number of matrix particles, along a path of increasing ρ_m and fixed fugacity of the adsorbate, z_a. In figure 3 results are shown for $z_a = 0.2, 1, 4, 10, 20, 60$ and for matrix densities in the range $\rho_m = 0$–0.25. Were the interaction between matrix particles that of hard bodies, $\rho_m = 0.25$ would correspond to close packing; the ideality, however, causes a void structure with non-zero free volume. The agreement is remarkably good up to $z_a = 10$ (corresponding to moderate adsorbate densities) in the entire range of ρ_m. At and above this

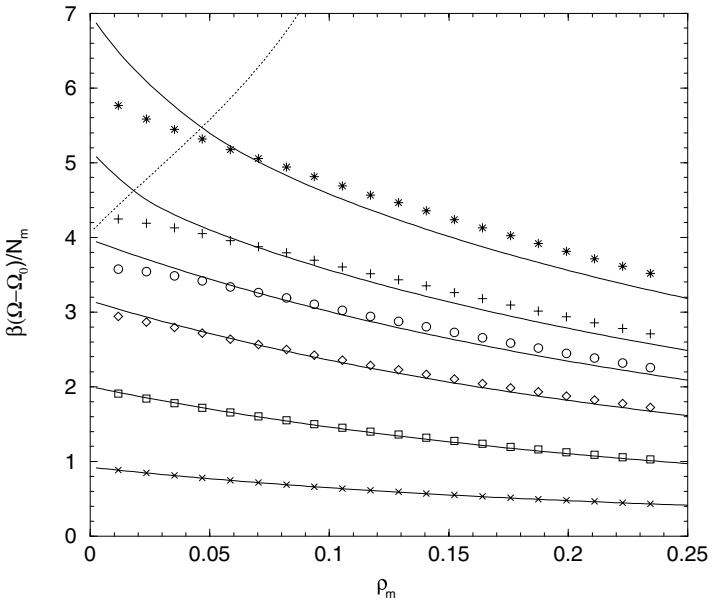

Figure 3. The change in grand potential, $\beta[\Omega - \Omega(\rho_m = 0)]/N_m$, due to the presence of matrix particles as a function of matrix density ρ_m for prescribed adsorbate fugacities $z_a = 0.2$, 1, 4, 10, 20, 60. Solid curves are from the QA DFT; the symbols are from treating the matrix as an external potential and averaging over explicit matrix configurations. Dashed curves depict the over-imposed phase diagram of figure 5 (adapted to represent the change in grand potential versus ρ_m).

value, deviations become more and more pronounced. Those occurring at low ρ_m are very significant: they may reveal the inherent inaccuracy of the external potential method due to the small system size.

Next we investigate the adsorbate density, ρ_a, for prescribed z_a and increasing ρ_m; results are shown in figure 4. The agreement is also good for z_a up to 10; above that value there are deviations for high matrix densities, $\rho_m > 0.1$, where the QA DFT over-estimates ρ_a.

Despite the discrepancies between the two approaches, we should acknowledge that the overall agreement is sufficiently good to take the QA functional seriously. Besides, we want to stress that it is not clear *a priori* which of the two methods is more accurate. It will be shown below by considering order parameters (figure 6) that considerable finite-size effects are present in the external potential method. Those may partly account for the discrepancy. It would be interesting to compare our results with those from computer simulations that would serve as a benchmark.

4.2. Phase diagram

Having thus gained confidence in the QA DFT, we will use it to calculate phase behaviour, which would be a challenging task with the external potential method. In the absence of the matrix, the LFMT predicts a second-order transition from a fluid phase to a columnar phase [12]. For small but non-zero ρ_m this continuous phase transition persists. In figure 5 the phase diagram is plotted as a function of ρ_a and ρ_m. For $\rho_m = 0$ the critical density and fugacity are $\rho_a^{crit} = (3 - \sqrt{5})/4 = 0.190\,98$ and $z_a^{crit} = (11 + 5\sqrt{5})/2 = 11.0902$ [12]. This result is compatible with that obtained by Bellemans and Nigam [18] using Rushbrooke

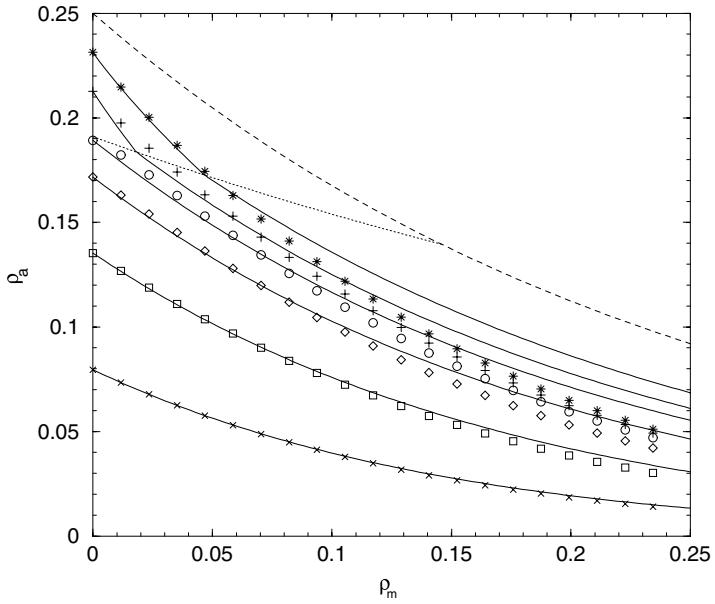

Figure 4. The adsorbate density ρ_a inside a porous matrix of density ρ_m for different adsorbate fugacities $z_a = 0.2$, 1, 4, 10, 20, 60. Solid curves indicate results from the QA DFT; symbols are from treating the matrix as an external potential. Dashed curves depict the over-imposed phase diagram of figure 5.

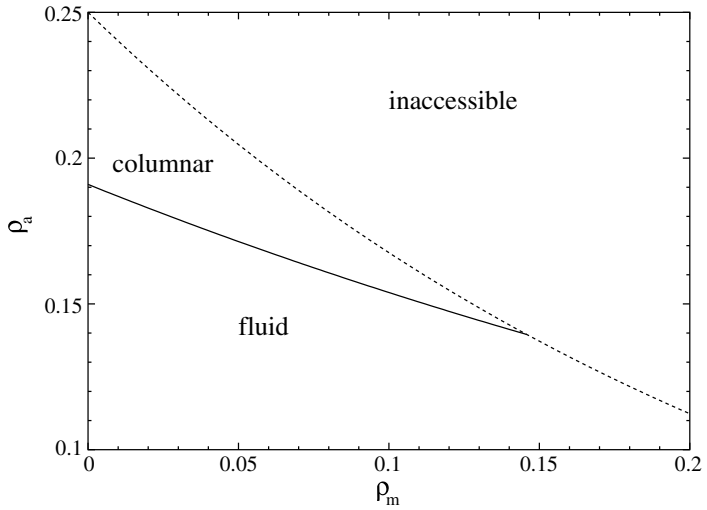

Figure 5. The phase diagram of hard squares of density ρ_a in a matrix of freely overlapping squares of density ρ_m. The solid curve indicates a continuous phase transition from fluid to columnar; the transition density ρ_a^{crit} is given by equation (18). The dashed curve indicates close packing, given by equation (20). Both curves meet at $\rho_m^* = 0.145\,80$, $\rho_a^* = 0.139\,53$; for larger ρ_m the fluid is the only stable phase.

and Scoins' method [23]. They also found a second-order transition but at slightly different parameters, namely $\rho_a^{crit} = 0.201\,75$ and $z_a^{crit} = 17.2878$.

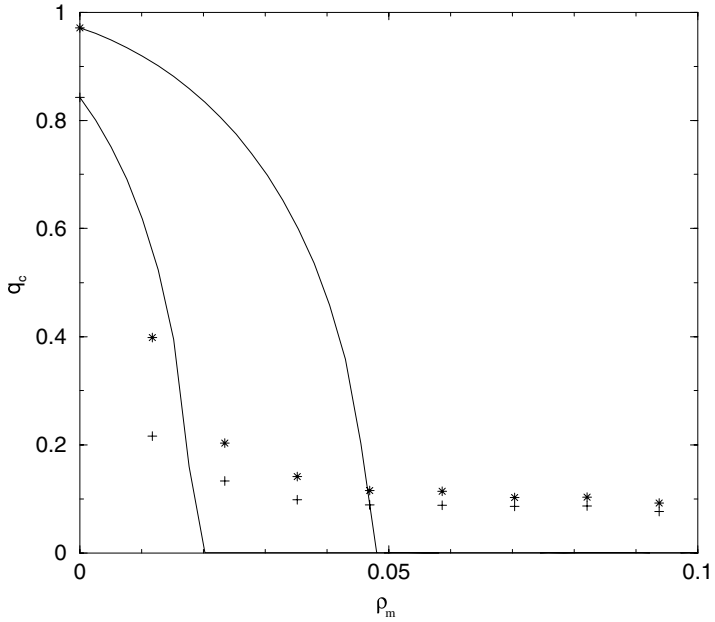

Figure 6. The columnar order parameter q_c of equation (21) computed for varying matrix density ρ_m and at constant adsorbate fugacity ($z_a = 20$ and 60). Curves are obtained from the QA density functional (top $z_a = 60$; bottom $z_a = 20$) and stars ($z_a = 60$) and pluses ($z_a = 20$) are the values computed with the random matrix approach averaged over 50 matrix realizations. Notice the strong finite-size effect in the fluid regions (where q_c should vanish).

The transition to a columnar phase can be studied by particularizing the functional (14) to a density profile which is uniform along columns that alternately take values ρ_1 and $2\rho_a - \rho_1$. The fluid phase corresponds to $\rho_1 = \rho_a$. The result is the free-energy density

$$\begin{aligned}\beta F V^{-1} = {} & \frac{\rho_1}{2}\ln\rho_1 + \left(\rho_a - \frac{\rho_1}{2}\right)\ln(2\rho_a - \rho_1) - \rho_a + \Phi_0(4\rho_m; 4\rho_a) \\ & - \Phi_0(2\rho_m; 2\rho_a) - \tfrac{1}{2}\Phi_0(2\rho_m; 2\rho_1) - \tfrac{1}{2}\Phi_0(2\rho_m; 4\rho_a - 2\rho_1) \\ & + \tfrac{1}{2}\Phi_0(\rho_m; \rho_1) + \tfrac{1}{2}\Phi_0(\rho_m; 2\rho_a - \rho_1),\end{aligned} \tag{16}$$

where V is the number of lattice sites (i.e. the system 'volume'). Minimizing with respect to ρ_1 leads to a third-degree polynomial in ρ_1, one of whose roots is ρ_a (corresponding to the fluid phase); of the other two, one is

$$\rho_1 = \rho_a + \sqrt{\frac{(\mathrm{e}^{-2\rho_m} - 2\rho_a)(\rho_a - \rho_a^{crit})(\frac{3}{2}\mathrm{e}^{-\rho_m} - \rho_a^{crit} - \rho_a)}{2\rho_a + (1 - \mathrm{e}^{-\rho_m})\mathrm{e}^{-\rho_m}}} \tag{17}$$

and the other one $2\rho_a - \rho_1$, where

$$\rho_a^{crit} = \tfrac{3}{4}\mathrm{e}^{-\rho_m}(1 - \sqrt{1 - (4/9)\mathrm{e}^{-\rho_m}}). \tag{18}$$

These two roots are real whenever $\rho_a^{crit} \leqslant \rho_a \leqslant \mathrm{e}^{-2\rho_m}/2$ (the upper bound is never reached because it is higher than the close-packed density; cf equation (20) below); this means that alternating columns have different densities, thus ρ_a^{crit} is the critical density of the continuous fluid–columnar transition.

Isofugacity curves are obtained as

$$z_a = \frac{(\mathrm{e}^{-2\rho_m} - 2\rho_a)^2 (\mathrm{e}^{-2\rho_m} - 2\rho_1)^2 \rho_1}{(\mathrm{e}^{-4\rho_m} - 4\rho_a)^4 (\mathrm{e}^{-\rho_m} - \rho_1)}, \tag{19}$$

where $\rho_1 = \rho_a$ for $\rho_a < \rho_a^{crit}$ and ρ_1 is given by (17) for $\rho_a \geqslant \rho_a^{crit}$; thus z_a^{crit} results from substituting $\rho_1 = \rho_a = \rho_a^{crit}$ in this expression. As $\rho_a \leqslant \rho_1 < 2\rho_a$ and $\mathrm{e}^{-\rho_m} \geqslant \mathrm{e}^{-4\rho_m}$, on increasing ρ_a the fugacity z_a diverges at

$$\rho_a^{cp} = \exp(-4\rho_m)/4, \tag{20}$$

the close-packed density. This result has a very clear physical meaning: $4\rho_a$ is the packing fraction of the adsorbate particles and $\exp(-4\rho_m)$ is the free volume left by the matrix particles; according to (20), close packing is reached when both are equal. This result is expected if the surface is negligible with respect to volume, so the true close-packed density must deviate from this prediction whenever the matrix consists of an ensemble of relatively small cavities.

The two curves $\rho_a^{crit}(\rho_m)$ and $\rho_a^{cp}(\rho_m)$ meet at $\rho_m^* = 0.145\,80$. This means that, for $\rho_m > \rho_m^*$, the columnar phase ceases to exist and only the fluid phase is stable. In order to understand the meaning of this special value of ρ_m we can relate it to the percolation threshold of the matrix. We do not know the precise value for this threshold, but we can check that of similar models: for 2×2 hard squares the estimated site percolation threshold is $\rho = 0.155$ [24], while a quarter of that of an ordinary lattice gas (squares occupy four sites) is $\rho = 0.148$ [25]. Both values are very close to ρ_m^*. This suggests that the disappearance of the fluid–columnar transition at this matrix density is associated with the splitting of the free volume left by the matrix into a disconnected ensemble of meso- and microscopic cavities within which the adsorbate is confined. Further investigations of the true percolation threshold for this particular matrix would be needed to settle this point.

Although we have not attempted to calculate the phase diagram using the external potential method, we have been able to check the phase that the system exhibits with the help of two order parameters. If we divide the lattice into four sublattices—such that sublattice 1 is formed by all sites, $\boldsymbol{s}$, with even s_x and even s_y; sublattice 2 by those with even s_x and odd s_y; sublattice 3 by those with odd s_x and odd s_y, and sublattice 4 by those with odd s_x and even s_y—and compute the average of the density in every sublattice, q_i ($i = 1, 2, 3, 4$), then the order parameters are defined as

$$q_c = \frac{1}{2\rho_a}\sqrt{|q_1 - q_3||q_2 - q_4|}, \tag{21}$$

$$q_s = \frac{1}{4\rho_a}|q_1 + q_3 - q_2 - q_4|. \tag{22}$$

Clearly, q_c is non-zero only in a columnar phase while it vanishes in the fluid and solid phases, and q_s is non-zero only in a solid phase while it vanishes in the fluid and columnar phases. Normalization is chosen so that $0 \leqslant q_{c,s} \leqslant 1$. These order parameters are also averaged over matrix realizations.

The first observation to be made is that both order parameters are affected by strong finite-size effects, so that they fluctuate around 0.1 when they should vanish. Apart from that, q_s is never found to increase anywhere in the phase diagram, while q_c rises rather close to the points where the fluid–columnar transition is predicted (see figure 6). The precise values of q_c in the columnar phase deviates from the analytical curves derived from the QA functional, but the region where this occurs is such a narrow gap in ρ_m and contains so few points that it is hard to tell how much of this deviation is due to the strong finite-size effect.

To give an illustration of what an ordered phase in a random matrix looks like, we present density profiles for the columnar phase in figures 2(c) and (d). In figure 2(c) the columns are

horizontal. Matrix particles generate a disturbance, mainly along the columns, which decays with distance.

We have confirmed the prediction of the external potential method that the solid phase is less stable than the columnar phase. To this purpose we have carried out an analysis similar to that performed for the columnar phase, but for a solid-like density profile. We have found that, for any $0 \leqslant \rho_m \leqslant \rho_m^*$, the solid—like the columnar—is more stable than the fluid for densities $\rho_a > \rho_a^{crit}$, but its free energy is larger than that of the columnar all the way up to close packing.

The location of the columnar phase with the help of the order parameters has allowed us to check for the existence of hysteresis. As in [3–5], for a given matrix density in the range $0 < \rho_m < \rho_m^*$ we have started off from a converged density profile at a low fugacity z_a and used it as the initial configuration to converge the density profile at a slightly higher z_a. We have iterated this procedure, making sure to be well in the columnar phase, and then repeated the whole process by decreasing z_a. For the convergence criterion from iteration step n to $n+1$ we used $\max_i |\rho_i^{(n+1)} - \rho_i^{(n)}| < 10^{-5}$. (Notice that Kierlik *et al* used $(1/N)\sum_i(\rho_i^{(n+1)} - \rho_i^{(n)})^2 < 10^{-8}$, which is milder than ours: the square root of this is less than 10^{-4} and there is an average over lattice sites; we take the worst case instead.) We performed this analysis at a single value of $\rho_m = 0.03$ where we are certain that, by increasing sufficiently the fugacity, the columnar phase is stable. We find that the two curves $\rho_a(z_a)$ thus obtained coincide, showing no sign of hysteresis. In the light of the study carried out in [3–5], this may be justified by the continuous character of the fluid–columnar transition of this model.

One final remark concerns the close packing. In figures 3 and 4 we have over-imposed the phase diagram obtained from the QA functional. Although the higher fugacity considered is $z_a = 60$, it is very clear that the close packing predicted by equation (20) strongly over-estimates that obtained from the external potential approach (for a few large values of ρ_m we have increased z_a up to 1000; the resulting values are very close to those obtained for $z_a = 60$—still very far from the close packing). It is not difficult to understand what happens. For (20) to hold, it is necessary that surface contributions are negligible compared to bulk contributions. But for large ρ_m the fluid is confined in an ensemble of (relatively small) cavities, so both contributions are comparable and (20) becomes a bad estimate for the close-packed density. The percolation threshold of the matrix is then an upper bound for the limit of validity of the QA functional, at least for high adsorbate densities.

5. Conclusions

In conclusion, we have considered the freezing of a hard-body lattice model in a porous medium. The latter is modelled as immobilized configurations of freely overlapping particles (or others—see appendix) which have the same size as the adsorbate particles. We have combined two recent density functional approaches to obtain the thermodynamics of the system via two routes. First, we treat the matrix as an external potential and minimize the free energy explicitly for many such matrix realizations. Subsequently, an explicit average over the different matrix realization is performed. The second route is direct via a DFT for mixtures of quenched and annealed species and gives the *average* free energy directly. The functional is constructed using the FMT recipe to generate a higher-dimensional theory from the 0D limit—an idealized situation where the many-body problem can be solved exactly. The second approach is computationally much simpler. We compare results for the free energy and the equation of state from both approaches and find reasonable agreement over a large density regime. Some deviations are apparent at high densities, but the overall agreement is quite good.

We note that the present combination of the lattice theory with the QA DFT indicates that the FMT is a flexible toolbox, where different components can be combined systematically.

For the present model we have not found any indications for the occurrence of hysteresis in sorption curves. We believe this is related to the fact that the model undergoes a continuous phase transition. The principal route that we followed in this work is applicable to other (also three-dimensional) lattice models [11, 12] that display first-order phase transitions. It would be interesting to address questions like hysteresis and the relation with the occurrence of metastable states in future work.

Acknowledgments

MS thanks Martin-Luc Rosinberg, Gilles Tarjus and Hartmut Löwen for useful discussions and acknowledges support from the Deutsche Forschungsgemeinschaft within the SFB TR6. The work of MS is part of the research program of the Stichting voor Fundamenteel Onderzoek der Materie (FOM), which is supported financially by the Nederlandse Organisatie voor Wetenschappelijk Onderzoek (NWO). LL's and JAC's work is part of the project BFM2000–0004 of the Ministerio de Ciencia y Tecnología (Spain).

Appendix. Construction of the quenched–annealed fundamental measure functional

The present lattice case allows us to make the construction of a QA fundamental measure functional more explicit than in the continuum case [13]. In the latter, one uses idealized 0D cavities, represented by delta-spike density distributions. On the lattice, however, one is able to treat cavities with varying shapes extending over several lattice sites (not just a single lattice site). Such cavities are still 0D, in the sense that placing two particles at arbitrary sites within the cavity induces pair overlap. We are led to consider such cavities due to the particular structure of the lattice fundamental measure functional (4): weighted densities are nothing but the probability of finding a fluid particle in the cavity defined by the diagrams, given that the density profile of the fluid is $\rho_a(\boldsymbol{s})$. In the following we make this fully explicit. This will allow us to also treat other pair interactions representing, alternatively to the ideal case, point and hard square matrix particles.

So let us start by considering a particular 0D cavity for the adsorbate, $\mathcal{C}$. As in [13], we must determine $p(\mathcal{C}) = \Xi_m(\mathcal{C})^{-1}$, the probability that the cavity is devoid of matrix particles, where $\Xi_m(\mathcal{C})$ is the grand partition function of the matrix particles in the cavity $\mathcal{C}$. A 0D cavity for the adsorbate does not mean a 0D cavity for the matrix particles: due to the different interaction potential, $\mathcal{C}$ may allocate more than one matrix particle at the same time. Once $p(\mathcal{C})$ is determined, the grand potential of the adsorbate in the cavity will be given by

$$\beta\Omega^{0d} = -p(\mathcal{C})\ln[1 + z_a(\mathcal{C})], \tag{A.1}$$

where $z_a(\mathcal{C}) \equiv \sum_{\boldsymbol{s}\in\mathcal{C}} z_a(\boldsymbol{s})$, with $z_a(\boldsymbol{s}) = z_a \mathrm{e}^{-\beta V_{ext}(\boldsymbol{s})}$ the 'local' fugacity of the adsorbate. From this,

$$\rho_a(\boldsymbol{s}) = -z_a(\boldsymbol{s})\frac{\delta\beta\Omega^{0d}}{\delta z_a(\boldsymbol{s})} = p(\mathcal{C})\frac{z_a(\boldsymbol{s})}{1 + z_a(\mathcal{C})}, \tag{A.2}$$

thus

$$z_a(\mathcal{C}) = \frac{\rho_a(\mathcal{C})}{p(\mathcal{C}) - \rho_a(\mathcal{C})} \tag{A.3}$$

where $\rho_a(\mathcal{C}) \equiv \sum_{\boldsymbol{s}\in\mathcal{C}} \rho_a(\boldsymbol{s})$, and

$$\beta\Omega^{0d} = -p(\mathcal{C})\ln p(\mathcal{C}) + p(\mathcal{C})\ln[p(\mathcal{C}) - \rho_a(\mathcal{C})]. \tag{A.4}$$

Therefore the excess free energy of the 0D cavity will be given by

$$\beta F_{exc}^{0d} = \beta\Omega^{0d} + \sum_{s\in\mathcal{C}}[\rho_a(s)\ln z_a(s) - \rho_a(s)\ln\rho_a(s) + \rho_a(s)] \tag{A.5}$$

$$= \Phi_0(p(\mathcal{C});\, \rho_a(\mathcal{C})), \tag{A.6}$$

where

$$\Phi_0(p(\mathcal{C});\, \eta) \equiv \eta + [p(\mathcal{C}) - \eta]\ln[p(\mathcal{C}) - \eta] - p(\mathcal{C})\ln p(\mathcal{C}). \tag{A.7}$$

As in equation (4), the functional will be given by

$$F_{exc}[\rho_m;\, \rho_a] = \sum_{s\in\mathbb{Z}^2}[\Phi_0(p(\,\cdot\,);\,\cdot\,_a) - \Phi_0(p(\,\cdot\,);\,\cdot\,_a) - \Phi_0(p(\circ\!-\!\circ);\,\circ\!-\!\circ_a) + \Phi_0(p(\circ);\,\circ_a)]. \tag{A.8}$$

The diagrams used as arguments of p are meant to denote the 0D cavities formed by the lattice nodes defining the corresponding weighted densities, cf equations (6)–(9).

It only remains to determine $p(\mathcal{C})$ in terms of $\rho_m(s)$ to complete the description. For that purpose we must compute $\Xi_m(\mathcal{C})$ for the three types of interaction potentials between matrix particles:

$$\text{(a) ideal:} \qquad V_{mm}(s) = 0, \tag{A.9}$$

$$\text{(b) points:} \qquad V_{mm}(s) = \begin{cases} \infty & \text{if } s_x = s_y = 0, \\ 0 & \text{otherwise,} \end{cases} \tag{A.10}$$

$$\text{(c) squares:} \qquad V_{mm}(s) = \begin{cases} \infty & \text{if } |s_x| < 2 \ \text{ and } \ |s_y| < 2, \\ 0 & \text{otherwise.} \end{cases} \tag{A.11}$$

In the ideal case (a),

$$\Xi_m(\mathcal{C}) = \mathrm{e}^{z_m(\mathcal{C})}, \qquad \rho_m(s) = z_m(s), \tag{A.12}$$

and therefore

$$p(\mathcal{C}) = \mathrm{e}^{-\rho_m(\mathcal{C})}. \tag{A.13}$$

In the points case (b),

$$\Xi_m(\mathcal{C}) = \sum_{N=0}^{|\mathcal{C}|} z_m^N Z_N(\mathcal{C}), \tag{A.14}$$

where $Z_N(\mathcal{C})$ is the partition function of N matrix particles in the cavity $\mathcal{C}$ made of $|\mathcal{C}|$ lattice sites. If we order these sites from 1 to $|\mathcal{C}|$, then this partition function is easily expressed as

$$z_m^N Z_N(\mathcal{C}) = \sum_{s_1<s_2<\cdots<s_N} z_m(s_1)z_m(s_2)\cdots z_m(s_N), \tag{A.15}$$

hence

$$\Xi_m(\mathcal{C}) = \prod_{s\in\mathcal{C}}[1 + z_m(s)]. \tag{A.16}$$

Now, from this grand partition function,

$$\rho_m(s) = \frac{z_m(s)}{1 + z_m(s)}, \qquad z_m(s) = \frac{\rho_m(s)}{1 - \rho_m(s)}; \tag{A.17}$$

therefore

$$p(\mathcal{C}) = \prod_{s\in\mathcal{C}}[1 - \rho_m(s)] = \mathrm{e}^{-\rho_m^*(\mathcal{C})}, \tag{A.18}$$

where we have made clear that $p(\mathcal{C})$ has the same expression as in the ideal case in terms of the new densities $\rho_m^*(\boldsymbol{s}) \equiv -\ln[1-\rho_m(\boldsymbol{s})]$. This makes sense if we take into account that the configuration of the ideal case corresponds to the configuration of this case with multiple occupancy of the sites. So, despite its higher complexity, this case maps trivially to the ideal case.

Finally, for the squares case (c), matrix and adsorbate particles have the same interaction potential, so

$$\Xi_m(\mathcal{C}) = 1 + z_m(\mathcal{C}), \qquad \rho_m(\boldsymbol{s}) = \frac{z_m(\boldsymbol{s})}{1+z_m(\mathcal{C})}, \qquad z_m(\mathcal{C}) = \frac{\rho_m(\mathcal{C})}{1-\rho_m(\mathcal{C})}, \tag{A.19}$$

and therefore

$$p(\mathcal{C}) = 1 - \rho_m(\mathcal{C}). \tag{A.20}$$

Substituting in (A.8) the expressions of $p(\mathcal{C})$ obtained for the two nontrivial cases (a) and (c), we end up with the expression (14), where $\Phi_0(\eta_m;\eta_a)$ is given by (15) for the ideal case (a) and by $\Phi_0(\eta_m;\eta_a) = (1-\eta_m-\eta_a)\ln(1-\eta_m-\eta_a) + \eta_a + \eta_m - (1-\eta_m)\ln(1-\eta_m)$ for the squares case (c).

References

[1] Gelb L D, Gubbins K E, Radhakrishnan R and Sliwinska-Bartkowiak M 1999 *Rep. Prog. Phys.* **62** 1573
[2] Evans R 1990 *J. Phys.: Condens. Matter* **2** 8989
[3] Kierlik E, Monson P A, Rosinberg M L, Sarkisov L and Tarjus G 2001 *Phys. Rev. Lett.* **87** 055701
[4] Kierlik E, Monson P A, Rosinberg M L and Tarjus G 2002 *J. Phys.: Condens. Matter* **14** 9295
[5] Rosinberg M L, Kierlik E and Tarjus G 2003 *Europhys. Lett.* **62** 377 (*Preprint* cond-mat/0206108)
[6] Thalmann F, Dasgupta C and Feinberg D 2000 *Europhys. Lett.* **50** 54
[7] Dasgupta C and Valls O T 2000 *Phys. Rev.* E **62** 3648
[8] Evans R 1992 *Fundamentals of Inhomogeneous Fluids* ed D Henderson (New York: Dekker) p 85
[9] Rosenfeld Y 1989 *Phys. Rev. Lett.* **63** 980
[10] Tarazona P and Rosenfeld Y 1997 *Phys. Rev.* E **55** R4873
[11] Lafuente L and Cuesta J A 2002 *Phys. Rev. Lett.* **89** 145701
[12] Lafuente L and Cuesta J A 2002 *J. Phys.: Condens. Matter* **14** 12079
[13] Schmidt M 2002 *Phys. Rev.* E **66** 041108
[14] Schmidt M, Schöll-Paschinger E, Köfinger J and Kahl G 2002 *J. Phys.: Condens. Matter* **14** 12099
[15] Frink L J, Salinger A G, Sears M P, Weinhold J D and Frischknecht A L 2002 *J. Phys.: Condens. Matter* **14** 12167
[16] Runnels L K 1972 *Phase Transitions and Critical Phenomena* vol 2, ed C Domb and M S Green (London: Academic) ch 8 p 305
[17] Burley D M 1972 *Phase Transitions and Critical Phenomena* vol 2, ed C Domb and M S Green (London: Academic) ch 9 p 329
[18] Bellemans A and Nigam R K 1967 *J. Chem. Phys.* **46** 2922
[19] Nisbet R M and Farquhar I E 1974 *Physica* **73** 351
[20] Slotte P A 1983 *J. Phys. C: Solid State Phys.* **16** 2935
[21] Ree F H and Chesnut D A 1967 *Phys. Rev. Lett.* **18** 5
[22] Lafuente L and Cuesta J A 2003 *Preprint* cond-mat/0306221
[23] Rushbrooke G S and Scoins H I 1955 *Proc. R. Soc.* A **230** 74
[24] Binder K and Landau D P 1980 *Phys. Rev.* B **21** 1941
[25] Stauffer D and Aharony A 1994 *Introduction to Percolation Theory* revised 2nd edn (London: Taylor and Francis)